Geomechanics and Engineering, *Vol. 32, No. 4 (2023) 375-385*
https://doi.org/10.12989/gae.2023.32.4.375

Dynamic mechanism of rock mass sliding and identification of key blocks in multi-fracture rock mass

Jinhai Zhao*[1,2,4,5], Qi Liu**[1,2], Changbao Jiang***[1,2], Zhang Shupeng[3], Zhu Weilong[1,2a] and Ma Hailong[1,2b]

[1]*State Key Laboratory Breeding Base for Mining Disaster Prevention and Control, Shandong University of Science and Technology,Qingdao 266590, China*
[2]*College of Energy and Mining Engineering, Shandong University of Science and Technology, Qingdao 266590, China*
[3]*Shandong Dongyue Energy Co., Ltd. Baizhuang Coal Mine,Taian, 271600, China*
[4]*Tsinghua Univ, State Key Lab Hydrosci & Engn, Beijing 100084, P. R. China*
[5]*Univ Queensland, Sch Earth Sci, Brisbane, Qld, 4072, Australia*

(*Received March 21, 2022, Revised January 13, 2023, Accepted January 16, 2023*)

Abstract. There are many joint fissures distributed in the engineering rock mass. In the process of geological history, the underground rock mass undergoes strong geological processes, and undergoes complex geological processes such as fracture breeding, expansion, recementation, and re-expansion. In this paper, the damage-stick-slip process (DSSP), an analysis model used for rock mass failure slip, was established to examine the master control and time-dependent mechanical properties of the new and primary fractures of a multi-fractured rock mass under the action of stress loading. The experimental system for the recemented multi-fractured rock mass was developed to validate the above theory. First, a rock mass failure test was conducted. Then, the failure stress state was kept constant, and the fractured rock mass was grouted and cemented. A secondary loading was applied until the grouted mass reached the intended strength to investigate the bearing capacity of the recemented multi-fractured rock mass, and an acoustic emission (AE) system was used to monitor AE events and the update of damage energy. The results show that the initial fracture angle and direction had a significant effect on the re-failure process of the cement rock mass; Compared with the monitoring results of the acoustic emission (AE) measurements, the master control surface, key blocks and other control factors in the multi-fractured rock mass were obtained; The triangular shaped block in rock mass plays an important role in the stress and displacement change of multi-fracture rock mass and the long fissure and the fractures with close fracture tip are easier to activate, and the position where the longer fractures intersect with the smaller fractures is easier to generate new fractures. The results are of great significance to a multi-block structure, which affects the safety of underground coal mining.

Keywords: dynamic response; key block; master control slip face; multi-fracture rock msss; numerical simulation

1. Introduction

Multi fracture rock mass is one of the most common engineering rock mass, which widely exists in underground engineering such as mining, petroleum, water conservancy and slope. (Bobet and Einstein 1998, Jalali *et al.* 2018, Castro *et al*. 2017, Cho 2007, Karatela *et al.* 2018, Wang *et al.* 2019, Xue *et al.* 2020, Zhou *et al*. 2020). In the process of geological history, underground rock mass has experienced complex geological processes such as fracture initiation, expansion, cementation and re expansion. Therefore, most rock masses exist in the form of rock block assemblages. The position and inclination of fracture surface and the shape of block in rock mass affect the failure and instability process of rock mass to a great extent, (Bobet and Einstein 1998, Feng *et al*. 2019a, Mahmoodzadeh *et al.* 2022), and then affect the safety of underground engineering. Therefore, it is of great significance to further study the sliding and instability of fractured rock mass (Blum *et al.* 2009, Gómez-Hernández *et al.* 2001, Hu *et al*. 2019, Shi Genhua 1977, Shi Genhua 1981).

Extensive engineering practices show that most failures of surrounding rocks occur in the form of block destabilization (Lawal *et al.* 2022, Ibishi *et al*. 2022, Rastegarnia *et al*. 2022). In particular, some blocks are slipped along the structural plane due to unloading after rock excavation, thereby influencing the stability of adjacent blocks, which in turn extends to a wide range of surrounding rock instability. Studying the shape and volume characteristics of blocks in multi fractured rock mass is of great significance for studying the instability mode of underground engineering and guiding the construction of engineering (Xie *et al*. 2006, Yang *et al.* 2004, Kim and Changani 2018, Varun and Eunhye 2017, Li *et al.* 2017, Lv *et al*. 2019, Zhao *et al.* 2022a).

∗Corresponding author, Professor
E-mail: Jinhai.zhao@sdust.edu.cn
**Dr.
E-mail: xihuancicuo@163.com
***Professor
E-mail: jcb@cqu.edu.cn
[a]Master
E-mail: zwl0315224@163.com
[b]Master
E-mail: 1766124758@qq.com

ISSN: 2005-307X (Print), 2092-6219 (Online)

The potential failure mode of a rock mass is often represented by the destabilization of rock blocks (masses) by cutting several structural planes and rock surfaces, appearing as the wedge slipping failure mode (Hoek *et al.* 2005, Yossef 2003, Kumsar *et al.* 2000, Jiang *et al.* 2013, Samanta and Sharma 2018). To investigate the instability failure mechanism of multi-fractured rock masses, a large number of studies have been performed. In these studies, the rock mass failure motion characteristics of the multi-fractured rock mass in near-fault mining were observed, and the risk of dynamic disaster hazards was analysed (Li *et al.* 2010, Katcoff.2014, Yang *et al*. 2011, Li *et al*. 2008, Meng *et al.* 2001). In other studies, the failure mechanism on the rock mass free face was examined (Yuan *et al.* 2012, Chen *et al.* 2011, Komurlu 2016). The shear-tension failure mode of rock mass on the free face was proposed, and the control method for controlling the stability of the exposed rock mass was presented. Additionally, the failure characteristics of the surrounding rock mass and the impact factors of multi-fractured rock mass failure based on the slip-line field theory were analysed in near-fault mining (Lisjak 2014, Yang *et al.* 2012, Liu *et al.* 2008, Zhao *et al.* 2022b). Mechanical analysis was performed to identify the range of failure hazards. The finite element method (FEM) was used to construct a methodology system for the identification of blocks, determination of the block mobility and mode of motion (Morgan 2017, Zhang *et al.* 2017, Sammis 1986, Xing *et al.* 2007). The evaluation of block stability and the analysis of block reinforcement offered a new possibility for studying the stability evolution of blocks under various complex conditions. The connectivity rate reduction method and stiffness reduction method were proposed to simulate the progressive failure process of rock blocks with a non-connected structural plane (Xiao *et al*. 2018, Xing *et al.* 2009, Tasdemir.1989). The method of block stability analysis considering the progressive failure process was established, and an extension from the qualitative analysis stage to the quantitative analysis stage was made(Vaziri *et al.* 2022, Ghyasvand *et al.* 2022).

The connectivity rate reduction method and the stiffness reduction method have been proposed to simulate the progressive failure process of the rock block bounded by the coplanar non-persistent joints, and a block stability analysis method considering the progressive failure process is established. The simulation of the progressive failure process has been helpful for the analysis of the deformation mechanism of the rock slope from the qualitative analysis stage to the quantitative analysis stage (Wang *et al.* 2016). Subject to the differences of the dip angle, block shape and other related factors, the motion process of a multi-fractured rock mass under stress is not coordinated, leading to nonlinear mutation process of the failure process. Considering the complexity of the composition of a multi-fractured rock mass, it is more important to investigate the master control surfaces and key blocks in the fracture rock mass system, identify the master control factors, and accordingly, take reasonable plans for reinforcement prevention and treatment (Zhao *et al.* 2018, Kim *et al.* 2019).

Numerous achievements have been presented in the formation and expansion of rock microfractures(Guo *et al.* 2017, Zhao *et al.* 2018). However, most studies are related to the effects of the expansion and failure of the rock mass fracture, while there is a lack of systematic studies on the identification, failure sequence and influence factors of key blocks in multi-fractured rock masses.

In this paper, based on three-directional stress-seepage testing, the whole process of rock mass crack initiation, expansion, cementation and redestruction is realized (damage-stick-slip process (DSSP)). Then, these results were compared and verified with the monitoring results of acoustic emission (AE) measurements. The master control surface, key blocks and other control factors in the multi-fractured rock mass based on the recemented multi-fractured rock mass system formed from the experimental process, the nonlinear friction finite element numerical analysis model was constructed using the PANDAS finite element numerical simulation software(Xing *et al.* 2007, Xing *et al.* 2009). The dynamic response process of the multi-fractured rock mass was investigated according to the distribution evolution law of the stress field and displacement field of the multi-fractured rock mass. This research is of great significance to the stability of rock mass affected by multiple fractures, the prevention and control of surrounding rock instability process and the identification of key blocks during coal mining.

2. Method and system of the fracture formation, expansion and recement experiments

2.1 Criterion of Damage-stick-slip Processes (DSSP)

There are many disordered fractures in a rock mass under natural conditions. Under stress action, a rock mass with natural fractures will be subject to cracking, crushing, granulation, recrystallization and the generation of cenotype minerals, ultimately forming a multi-fractured rock mass with a certain rock fabric. Rock materials continuously fail under mine pressure action, thus forming joints and fractured surfaces at different scales. In addition, these materials slip along the existing structural plane, which facilitates the generation of a joint fracture surface. In a multi-fractured rock mass, the structural plane, which plays an important role in mechanical control, is referred to as the “master control slip face”. When the frictional force on the slip face is insufficient to maintain the stability of the structural surface, slip motion of the structural plane occurs. To investigate the effects of the mechanical properties of rock materials in a rock mass, the contact face nature and dig angle of the fracture surface on the formation of a new structural plane in the rock mass and the order of activation on the old fracture plane, a mechanical analysis model, as shown in Fig. 1, was established.

$$P_1 = q_1 L_1 \tag{1}$$

$$P_2 = q_2 L_2 \tag{2}$$

$$\varphi = \frac{\pi}{2} - \theta \tag{3}$$

In this paper, the DSSP model was constructed based on a single slope. In the presence of a single slope

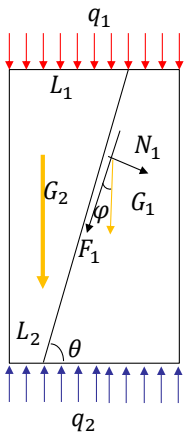

(a) Mechanical model of single-fracture surface

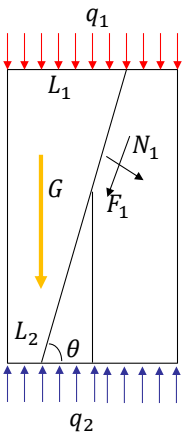

(b) Mechanical model of multi-fractures surface

Fig. 1 Single-fracture and multi-fractures DSSP mechanical model

$$F_1 = (G + q_1L_1 - q_2L_2)\cos\theta \tag{4}$$

$$N_1 = (G + q_1L_1 - q_2L_2)\sin\theta \tag{5}$$

$$T_1 = (CL_1\sec\theta + N_1\tan\varphi) \tag{6}$$

$$D = F_1 - T_1 \tag{7}$$

where P1 is the upper load, P2 is the lower load; φ is the angle between the slope and the vertical direction; F1 is the slipping force of the shear plane; T1 is the shear resistance on the slope; and D is the failure stress difference.

According to the Mohr-Coulomb strength theory, the surface failure criterion can be expressed as the difference between the slipping force F_1 along the shear surface and the shearing resistance T_1 on that surface. If this value is greater than 0, then the coal wall will be subject to shear failure, i.e.

$$D = F - T \tag{8}$$

$$D_1 = (G + q_1L_1 - q_2L_2)\cos\theta\text{-}(CL_1\sec\theta + N_1\tan\varphi) \tag{9}$$

where θ is the angle between the fracture surface and the horizontal plane; φ is the internal friction angle in the rock; L_1 and L_2 are the lengths of the upper and lower sections on the fracture surface, respectively; q_1 and q_2 are the pressures of the upper and lower sections on the fracture surface; G is the gravity; and C is the cohesion of the rock.

If the rock mass is absent from the weak plane, then the criterion for failure is

$$D = F - T = \begin{cases} \geq 0 \rightarrow \text{With shear failure} \begin{cases} F \leq F_\mu & Stick \\ F \geq F_\mu & Slip \end{cases} \\ \leq 0 \quad \text{Without shear failure} \end{cases} \tag{10}$$

In the presence of a weak plane in the rock mass, the judgement criteria differ greatly. When the specimen is an intact rock mass, the relationship between the shear stress and shear strength should be judged first; when the shear stress is less than the shear strength, new failure will no longer be generated. In this case, the relationship between the frictional force and shear stress is dominant. When the shear stress is greater than the shear strength, a new fracture face will take form. In this case, this face may move along the formed shear surface and the original shear surface, which can be controlled with specific values.

$$\text{D=max}\left\{ \begin{array}{c} F - T = \begin{cases} \geq 0 \\ \leq 0 \end{cases} \rightarrow \text{New contact face} \begin{cases} F \leq F_\mu & Stick \\ F \geq F_\mu & Slip \end{cases} \\ \begin{array}{cc} F \leq F_\mu & Stick \\ F \geq F_\mu & Slip \end{array} \end{array} \right\} \tag{11}$$

The setup was configured according to the above equation before fracture formation. In the velocity-dependent frictional contact, the slipping process of the fault can be classified into stick and slip. Based on Coulomb's friction law, the frictional force applied on the central contact face during contact can be described as (Xing *et al.* 2007)

$$f_m = E_t\overline{u}_m^e = E_t\sum\Delta\overline{u}_m^e \qquad \text{(Stick)} \qquad F \leq F_\mu \tag{12}$$

$$f_m = \epsilon_m\overline{F} \qquad \text{(Slip)} \qquad F \geq F_\mu \tag{13}$$

Where

$$\epsilon_m = f_m^e/\sqrt{f_l^e f_l^e}, f_m^e = E_t\left(\overline{u}_m - \overline{u}_m^p \mid_0\right) \tag{14}$$

where f_m (m=1, 2) is the frictional stress component along the tangential direction; E_t is the parameter along the tangential direction; and $\Delta\overline{u}_m^e$ and $\Delta\overline{u}_m^p$ are the relative displacement increments under the stick state and slip state, respectively. $\overline{F}$ is the frictional force, $(\overline{F} = \mu f_n)$ where μ is the friction coefficient, $(\mu = \mu(f_n, \tilde{u}_{eq}^{sl}, \varphi_1, T))$ and f_n is the normal contact force. The parameter $\tilde{u}_{eq}^{sl}$ is the equivalent tangential velocity; φ is the state variable; T is the temperature; l, m=1, 2, i, j, k=1, 2, 3; and F_μ is the max. static friction.

The experimental findings proved (Xing *et al.* 2009) that the variation in the frictional force is closely related to the friction velocity during the friction process of the rock mass

$$\tau = F(V, \mathrm{f}_n, \varphi_1, \varphi_2, \cdots, \varphi_n) \tag{15}$$

$$\frac{d\varphi_i}{dt} = G_i(V, \mathrm{f}_n, \varphi_1, \varphi_2, \cdots, \varphi_n), i = 1, n \tag{16}$$

Table 1 Basic mechanical parameters of specimen and the amount of grouting

Specimen number	Lithology/mixture ratio(cement:quartz sand:gypsum)	Length/mm	Width/mm	Height/mm	Weight before grouting /kg	Weight after grouting/kg	amount of groutin/kg
4-1	2:1:1	150.12	150.13	300.15	14.34	14.75	0.41
4-2	2:1:1	150.13	150.05	300.02	14.85	15.33	0.48
5-1	2:6:1	150.08	150.07	300.33	14.28	14.90	0.62
5-2	2:6:1	150.06	150.06	300.11	14.15	14.94	0.79
6-1	2:8:1	150.11	150.12	300.09	13.46	14.41	0.95
6-3	2:8:1	150.10	150.10	300.15	13.34	14.25	0.91

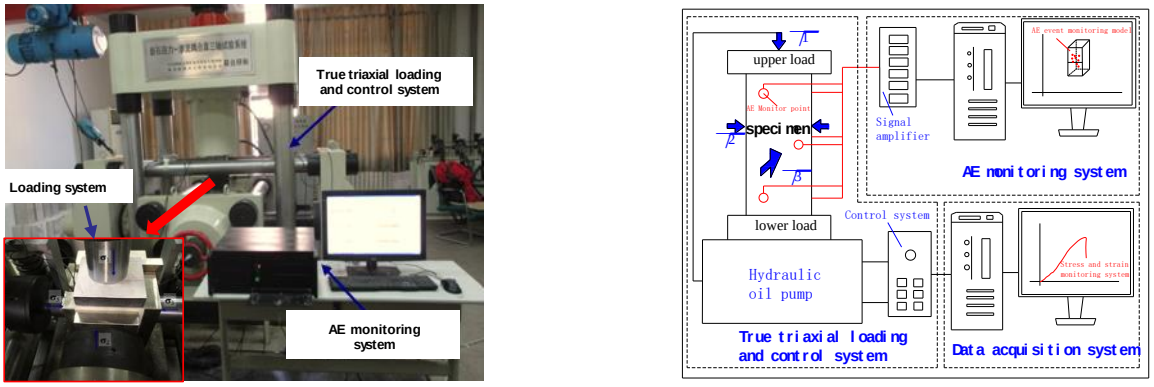

(a) True triaxial testing machine (b) System schematic diagram

Fig. 2 True triaxial testing machine load control system and monitoring system

Under the transient state, the slip velocity-dependent frictional force can be described as

$$\tau = f_n\left(\mu_0 + \varphi + aln\left(\frac{V}{V_{ref}}\right)\right), \frac{d\varphi}{dt} = -\left[\left(\frac{V}{L}\right)\left(\varphi + bln\left(\frac{V}{V_{ref}}\right)\right)\right] \quad (17)$$

Under a steady state, the frictional force can be expressed as

$$\tau^{ss} = f_n(\mu_0 + (a-b)\ln(\frac{V}{V_{ref}})) \quad (18)$$

where $a = V(\partial\tau/\partial V)_\varphi/f_n = (\partial\tau/\partial lnV)_\varphi/f_n$; $a-b = (d\tau^{ss}/dlnV)/f_n$; a and b are empirical parameters; a is the transient sensitivity; a-b is the long-term velocity sensitivity (positive/negative value determines the velocity enhancement and reduction in the frictional slip); L is the critical slip distance; V_{ref} and V are the reference velocity and velocity at anytime point, respectively; and μ_0 is the friction coefficient at the reference velocity of V_{ref}.

When multiple cracks exist, the instability form is similar to that of a single crack, which is mainly determined by the relationship between sliding force F and shear T. The determination method refers to the formula 11.

2.2 Experimental loading system and monitoring equipment

The fractured rock mass in nature will be cemented again in the long-term geological process. In engineering, the fractured rock mass will also be cemented through thecementing material.Therefore, it is of great significance to study the cementation characteristics of fractured rock mass (Wang *et al.* 2018, Liu *et al.* 2008). The failure form of specimen 4-1 is similar to that of the established theoretical analysis model, so this paper takes specimen 4-1 as an example. In order to ensure the homogeneity of rock mass, rock-like materials are used for the test. In this study, the ratio of specimen 4-1 (cement(28 day strength of cement is 42.5 MPa): quartz sand: gypsum) was 2:2:1, and the specimen was prepared using an in-house test mould, The uniaxial compressive strength of the sample is about 25 MPa. The loading on the specimen and the monitoring of specimen failure were performed with a loading rig, and the monitoring equipment was based on an in-house rock-stress-seepage coupling true triaxial experimental system and a MISTRAS series PCI-2 AE system. The elastic modulus of test piece 4-1 is 8×10^9Pa, Poisson's ratio is 0.35 and cohesion is 6×10^5Pa. A three-directional load was applied at the same time, and the loading process stopped if the specimen failed. The specimen parameters is shown in Table 1. The crack propagation was monitored dynamically in real time with the AE monitoring system. In this experiment, 6 channels were designed, and three-dimensional monitoring was performed on the specimen. Data acquisition and real-time display were enabled with AEwin software. A schematic diagram of the true triaxial loading control and AE monitoring system is shown in Fig. 2.

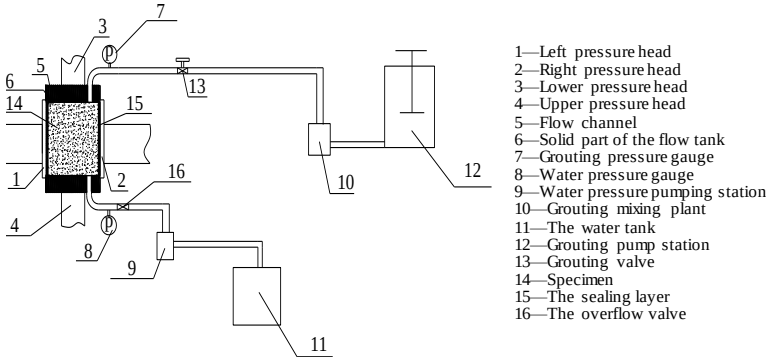

Fig. 3 Schematic diagram of the three-direction stress-seepage coupling grouting test system

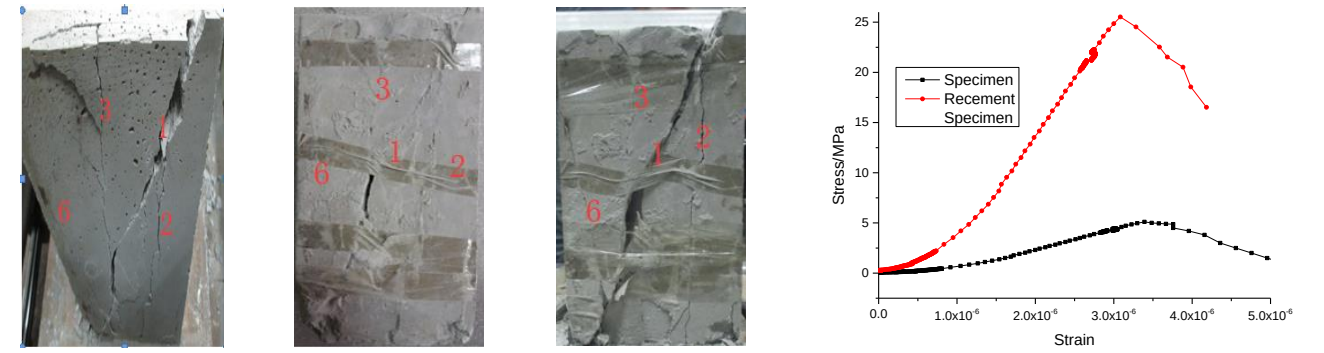

(a) Fracture formation (b) Recement specimen (c) Re-failure of the recemented specimen (d) Stress-strain curves of the recemented combination rock mass

Fig. 4 Fracture zone formation and recemented rock specimen failure process (note: No.1,2,3and 6 in Figs. (a)-(c) the number of rock blocks)

2.3 Experimental system and method of recement multi-fractured rock mass

The studies on the identification and failure sequence of key blocks in multi-fractured rock masses is not enough. In this paper, based on three-directional stress-seepage testing, the whole process of rock mass crack initiation, expansion, cementation and redestruction is realized (damage-stick-slip process (DSSP)). The three-direction stress-seepage coupling grouting test system is shown in Fig. 3. This experimental unit can be used to grout the specimen with the constant pressure of the surrounding rock and conduct failure tests over the recemented rock mass after grouting, which tends to be closer to the grouting and failure process in a real rock mass. The experimental method is described below: (1) In the first step, a confining pressure is applied, axial loading is applied to the specimen after it reaches the desired value, and the rock specimen failure is monitored under stress. (2) Until the rock specimen fails, the confining pressure is kept constant, and the grouting pressure and grout of the failed rock specimen are adjusted. (3) The confining pressure constant is kept constant until the grouting cement reaches the desired strength, axial loading is continuously applied to the specimen, and a quantitative analysis of the specimen strength after grouting is performed.

Then, these results were compared and verified with the monitoring results of acoustic emission (AE) measurements.

The master control surface, key blocks and other control factors in the multi-fractured rock mass. The dynamic response process of the multi-fractured rock mass was investigated according to the distribution evolution law of the stress field and displacement field of the multi-fractured rock mass. This research is of great significance to the stability of rock mass affected by multiple fractures, the prevention and control of surrounding rock instability process and the identification of key blocks during coal mining.

3. Experimental results

3.1 Multi-fracture model and recement experiment

The true triaxial experimental system was used to implement independent servo control over the three-dimensional stress, with a maximum vertical load of 1600 kN and a maximum lateral load of 960 kN. The loading process was performed with a true triaxial test unit. The three-directional stress load was up to the intended confining pressure of 1 MPa. The confining pressure value was maintained, the axial pressure was continuously loaded at a velocity of 0.2 kN/s, and the loading process stopped until the specimen formed connected cracks. Fig. 4 shows the fracture zone formation (a); the fracture zone recement (b) and the failure process of the recementing (c) of Specimen 4-1. For the purpose of this experiment, the first

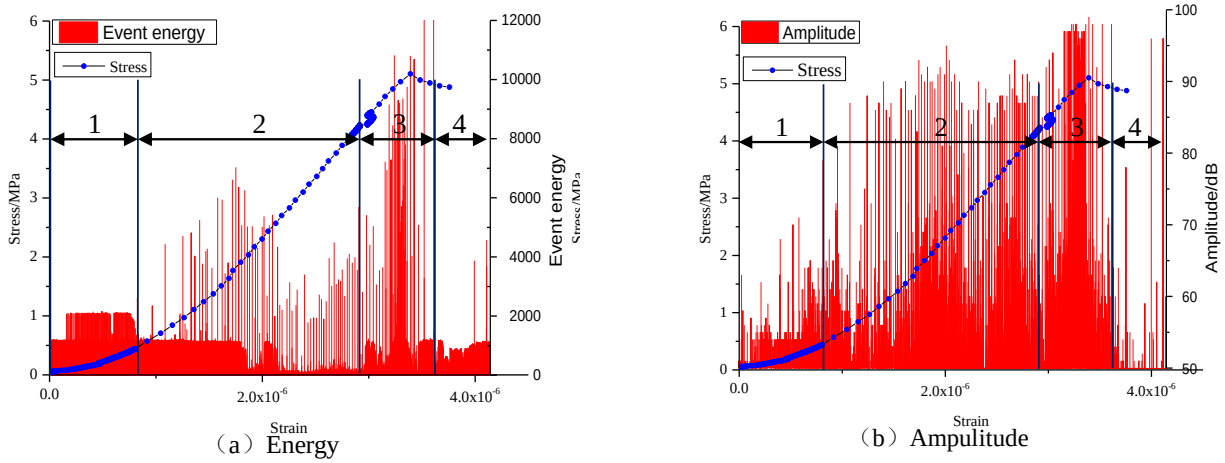

（a）Energy （b）Ampulitude

Fig. 5 Acoustic emission energy and amplitude change about the recemented rock specimen 4-1
(Note: 1-Compaction stabilization stage; 2-Low-amplitude failure stage; 3-High-amplitude failure stage; 4-Low-amplitude slip stage)

step aimed at forming a connected fracture failure zone and providing experimental conditions for the grouting and recementing of the fracture zone in the next step. Therefore, the experiment stopped after the entire connected fracture was formed, and the stress-strain curves with respect to the loading process of the specimen are shown in Fig. 4(d). The recemented fracture zone experiment was carried out over the above multi-fractured rock mass. In this paper, a typical grouted rock mass was selected for analysis, and the grouted specimen and re-failure mode are shown in Fig. 4(d).

A large fracture zone (#1) and two small fracture zones (#2 and 3) were formed after the specimen was loaded. The specimen was mainly subject to shear compression failure. After the specimen was grouted, the grouting effect turned out to be effective (b), and the fracture cementation rate was over 90%. During the loading process of the recemented fracture rock mass, the included large fracture numbered #1 was the master slip face. The small fracture zone numbered #2 was also subject to activation, but no large-scale failure was formed. The original fracture position numbered #3 was not subject to activation, but a new fracture zone was formed at the #6 position and was connected to the large fracture 1, leading to instability of the boundary block. The core zone blocks between #1 and #2 were not subject to activation during the failure process. The failure order was recorded in the experiment process. The new fracture compression failure first occurred at #2, with the loading of axial force. The upper part of the #1 large fracture position was subject to activation and ultimately led to slip, and the new fracture propagation that occurred at 2 stopped. However, during the slip process of the fracture at #1, a new fracture occurred at #6 and was ultimately connected with the large fracture at #1. In summary, the damage-cement-redamage process of rock mass was accompanied by the formation of new fractures and the activation process of the cement fractures. This process matched the mechanical model constructed in Eq. (11). The recemented rock mass was subject to new failure, but the slip motion caused by the large fracture surface dominated, and the instability process of the multi-fractured rock mass was attributed to the combined action of propagation of new fractures and the activation motion of existing fractures.

3.2 Acoustic emission characteristics of the recement zone experiment of the fractured rock mass

The advantages of AE include real-time monitoring and long-term monitoring of crack propagation, which contribute to revealing the process of crack initiation, expansion and coalescence and also reflect the fracture position and sequence of the specimen. The process of rock damage and recemented rock mass failure is accompanied by energy accumulation and release. The rapid energy release process will lead to the occurrence of AE events, which can effectively capture the rock mass activation, slip sequence, activation damage of recemented rock mass andother time-dependent characteristics. AE monitoring data include the rise time, count, energy, duration, amplitude, and peak frequency. In this paper, the amplitude, energy and number of AE events were considered as main references to reveal the intrinsic relationship between the damage activation process and the energy change during the process of recement failure, as well as the main factors controlling the occurrence of activation and failure.

The AE test results of Specimen 4-1 are shown in Fig. 5. In this paper, the specimen was analysed with reference to the amplitude and energy change in Channel 2. The energy and amplitude curves are shown in Figs. 5(a) and 5(b), respectively. Specimen 4-1 of the recemented rock mass was mainly divided into four stages during the slip failure process, i.e., the compaction stabilization stage, low-amplitude failure stage, high-amplitude failure stage, and low-amplitude slip stage. In the stabilization stage, the energy value was smaller, the maximum AE energy value was 200, and the distribution was relatively uniform. In this stage, the amplitude of the AE event was also smaller, and the compaction process of the recemented specimen and the friction process between the specimen and hydraulic head during the compression process were dominant.

Fig. 7 shows the stress change process along the vertical direction. The stress distribution was relatively uniform

Fig. 6 Multi-fracture system analysis model and monitoring point arrangement

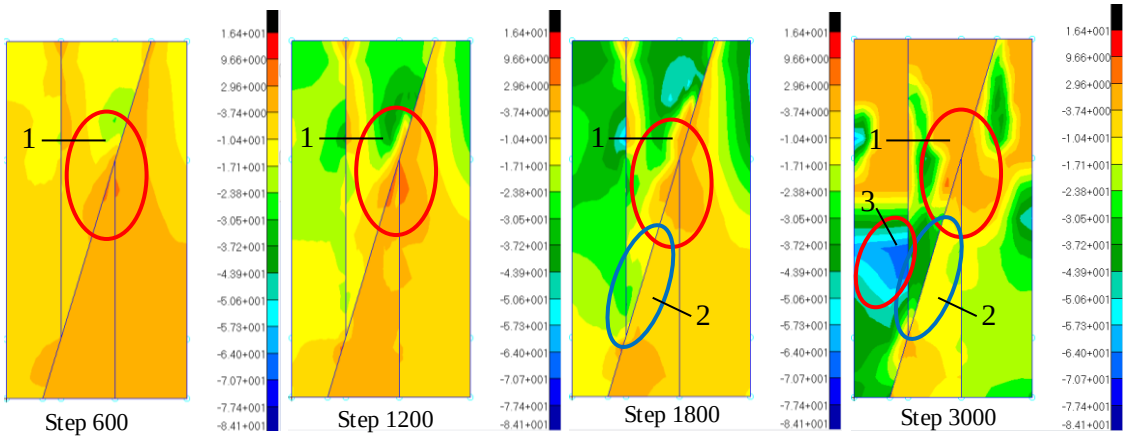

Fig. 7 Vertical stress(σ_y) change of stress concentration area

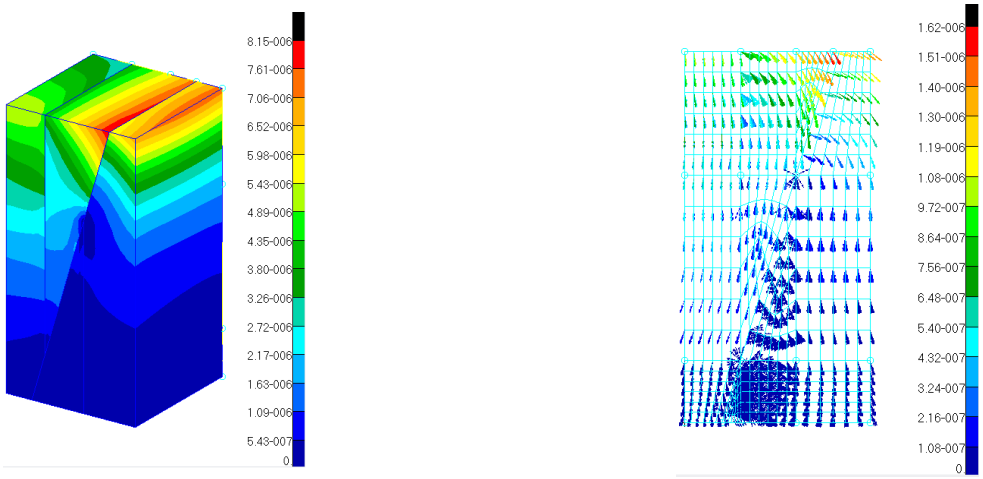

Fig. 8 Rock block movement speed change variation diagram and the direction of motion

during the initial loading stage (as shown by step 600 in Fig. 7). Before the joint began to slip, the stress distribution was always under this common change state, indicating that the stress change process was the same as the stress change law of the intact rock mass. As the stress loading was further applied, the stress difference between different blocks began to appear, and the high stress concentration zone was first formed in Block 2. Many joints in Contact Faces 1 and 2 changed from stick to slip, and the unevenness of the stress distribution further increased. Block 2 slipped along Vertical Plane 1 and Slope 2. The uneven distribution of local stress also led to discontinued block motion and in turn impacted the stress (energy) release process along the contact surface.

As Block 2 moved obliquely downward along Slope 2, the stress concentration zone was transferred to Block 1 and formed a stress concentration zone with Block 1 at the tip of Block 2. With the formation of a local stress concentration

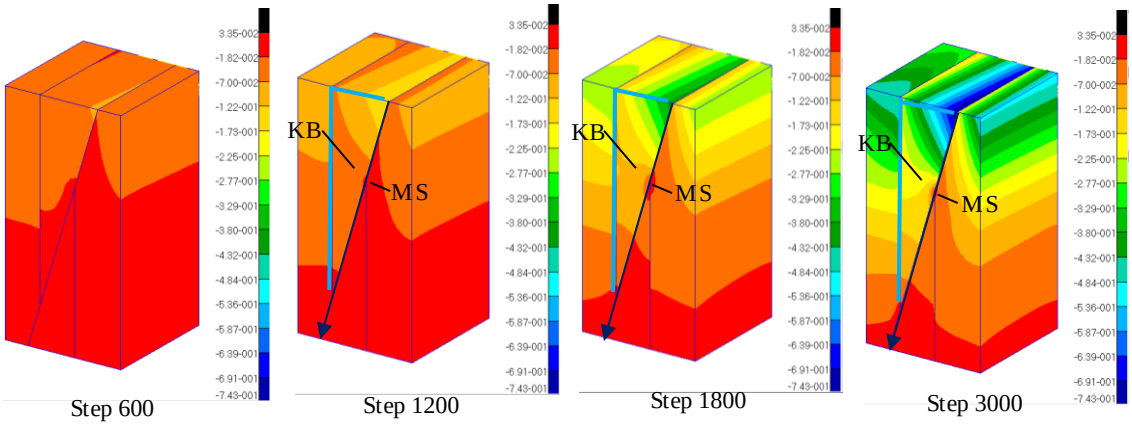

Fig. 9 Rock block displacement change
(Note: KB means Key Block; MS means Master Surface)

zone, the joint under the stick state also entered the slip state after being pushed by the slipping joints near the slip surface, leading to a sudden change in the slipping velocity and a rapid failure of the specimen, as shown in Fig. 8. This change process matched the process recorded in the experiment and the AE monitoring process, which verified that the numerical stimulation was correct.

Figs. 9-11 show the displacement change process of the proposed model at different time points and the motion direction and the monitoring point displacement change. The displacement change law helps visualize the motion differences between blocks. At the initial loading time, the displacement was basically the same between blocks, indicating that different blocks still maintained coordinated motion with increasing axial force. As the axial force further increased, the overall displacement when loaded at Step 1200 ranged from -1.8×10^{-2} mm to -7×10^{-2} mm. When the force was loaded at Step 1800, the displacement difference between blocks began to appear, and the maximum displacement was up to 1.73×10^{-1} mm. When the force was calculated at Step 3000, the maximum displacement was up to -7.43×10^{-1} mm. Taking the top interface of the specimen as an example, the maximum displacement difference between block 1 and 3 was 2.3 and 1.4 times, respectively.

4. Discussion

According to the above experimental findings, the recemented rock mass failure was mainly subject to the inclined fracture surface and the wedge motion (Jalali *et al.* 2018, Karatela *et al.* 2018, Wang *et al.* 2019). With the presence of a triangular wedge block, the fracture face at both ends and the top of the wedge block were the key positions where slip failure and stress concentration occurred (Xing *et al.* 2007).

It is difficult to obtain the shear force on the fracture surface in the rock mass during the true triaxial test, Acoustic Emission is used to monitor the internal failure process of the specimen. According to the distribution of AE events at different time points, the fracture zone was

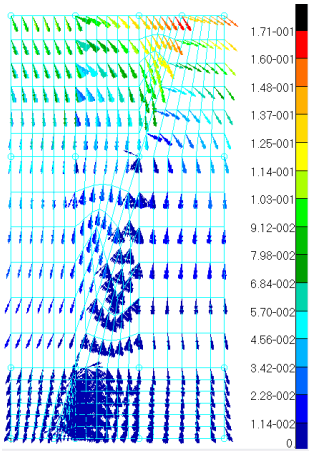

Fig. 10 Vector illustration of the rock block diagram

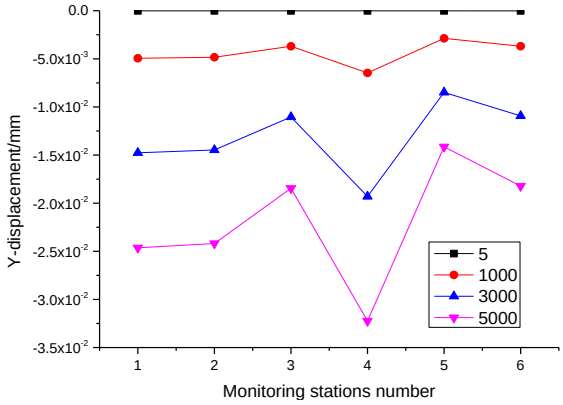

Fig. 11 Monitoring point displacement change displacement direction

first concentrated in the #1 zone, as shown in Fig. 12, followed by many failures in the #2 zone, as shown in Fig. 12, while the increase in failures in the #1 zone was less. As the axial force was further loaded, new fracture zones were mainly concentrated at #3 Point. This process matched the failure zone formation process and the fracture zone, as indicated in the experimental record of Fig. 4, and the stress evolution process of the “passive wedge block”, as shown in Fig. 7.

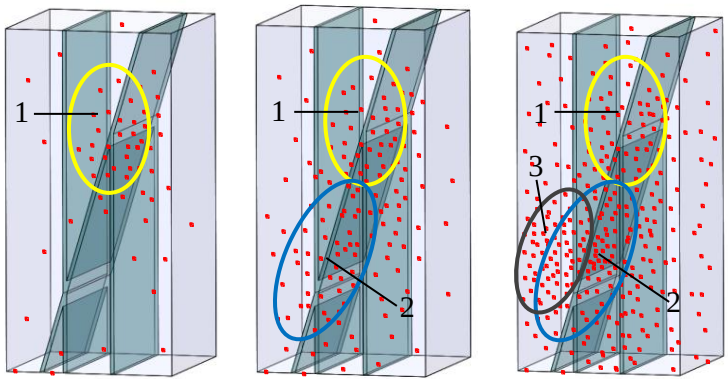

Fig. 12 Monitoring results of AE events at different time and change of AE events concentration area

Given the stress, velocity and displacement change process, the dig angle of the block played a crucial role in the slipping process. In the proposed model, the stress concentration zone was dominated by the development of Inclined Wedge 2 to the left free face direction of Block 1, and the maximum displacement position occurred where the upper part of Wedge 2 came into contact with the inclined slope. In summary, the motion of the “isolated wedge” that was similar to the #2 Wedge had a significant effect on the stability of the multi-fractured rock mass system, and the slipping block motion in turn impacted the stress and displacement change process of the non-slipping block. In this sense, similar "passive wedges" were considered the critical positions prone to disasters, so key monitoring should be performed.

5. Conclusions

(1) In this paper, the process of rock mass crack initiation, expansion, cementation and redestruction is realized by experimental analysis and numerical simulation. The rock mass DSSP mechanical analysis model was established to derive the coordination and correlation between the formation of new fractures and the slipping of existing fractures. The results show that the "stress-seepage coupling grouting experimental system" allowed for in situ seepage coupling, grouting reinforcement strength, and safety test processes.

(2) The numerical model for a multi-fractured rock mass was established to analyse the failure law of a recemented rock mass, which was verified with the results obtained from the mechanical experiment and AE monitoring. The results show that the initial fracture angle and direction had a significant effect on the re-failure process of the cement rock mass.

(3) The criterion for judging the key blocks and master control slip face was established by a numerical simulation method. The maximum displacement occurred in the upper part of the triangular passive wedge during the motion along the inclined surface, and the stress concentration occurred at the lower part of the tip, which was the key block that should be detected in particular. The long fissure and the fractures with close fracture tip are easier to activate, and the position where the longer fractures intersect with the smaller fractures is easier to generate new fractures.

Expectation

(1) Due to the theoretical model of multi-fracture rock mass is relatively complex, this paper only analyzes the process of damage-stick-slip when a single fracture exists. According to the key block identification methods and identification factors obtained in this paper, the later work is to establish the theoretical analysis model of multi-fracture rock mass.

(2) The acoustic emission(AE) part judges the order of block slip according to the sequence of acoustic emission events. In the follow-up work, the slip results need to be corrected in combination with theoretical analysis to verify the accuracy of experimental and theoretical results.

Acknowledgments

This study was funded by National Natural Science Foundation of China (52104203), Shandong Province Natural Science Foundation Project (ZR2020QE128, ZR2020ME102, ZR2021ME138).

Conflict of Interest

The authors declare that they have no conflict of interest.

References

Blum, P., Mackay, R., Riley, M.S., Finkel, M., Barcelo, D., Barth, J.A.C. and Grathwohl, P. (2009), “Stochastic simulations of regional scale advective transport in fractured rock masses using block upscaled hydro-mechanical rock property data”, *J. Hydrology*, **369**(3), 318-325. https://doi.org/10.1016/j.jhydrol.2009.02.009.

Bobet, A. and Einstein, H.H. (1998), “Fracture coalescence in

rock-type material under uniaxial and biaxial compression", *Int. J. Rock Mech. Min. Sci*., **35**(7), 863-888. https://doi.org/10.1016/S0148-9062(98)00005-9.

Castro-Filgueira, U., Alejano, L.R., Arzúa, J. and Ivars, D.M. (2017), "Sensitivity analysis of the micro-parameters used in a PFC analysis towards the mechanical properties of rocks", *Proc. Eng*., **191**, 488-495. https://doi.org/10.1016/j.proeng.2017.05.208.

Chen, L., Meng, X., Gao, Z., Wang, X. and Jin, J. (2011), "Analysis on spalling mechanism of coal wall law for fully mechanized high cutting coal mining face", *Coal Sci. Technol*., **39**(5), 18-24.

Cho, N., Martin, C.D. and Sego, D.C. (2007), "A clumped particle model for rock", *Int. J. Rock Mech. Min. Sci*., **44**(7), 97-1010. https://doi.org/10.1016/j.ijrmms.2007.02.002.

Feng, F., Li, X.B., Rostami, J., Peng, D.X., Li, D.Y. and Du, K. (2019a), "Numerical investigation of hard rock strength and fracturing under polyaxial compression based on Mogi-Coulomb failure criterion", *Int. J. Geomech*., **19**(4), 040190051. https://doi.org/10.1061/(ASCE)GM.1943-5622.0001352.

Ghyasvand, S., Fahimifar, A., Nejad, F.M. (2022), "On the optimum design of reinforcement systems for old masonry railway tunnels", *Geomech. Eng*., **28**(2), 145-155. https://doi.org/10.12989/gae.2022.28.2.145.

Gómez-Hernández, J.J., Hendricks Franssen, H.J. and Cassiraga, E.F. (2001), "Stochastic analysis of flow response in a three-dimensional fractured rock mass block", *Int. J. Rock Mech. Min. Sci*., **38**(1), 31-44. https://doi.org/10.1016/s1365-1609(00)00062-9.

Guo, W., Zhao, J., Yin, L. and Kong, D. (2017), "Simulating research on pressure distribution of floor pore water based on fluid-solid coupling", *Arabian J. Geosci*., **10**, 1-14. https://doi.org/10.1007/s12517-016-2770-6.

Hadi, H., Alireza, K. and Mohammad, F.M. (2015), "Fracture analyses of different pre-holed concrete specimens under compression", *Acta Mech. Sin*., **31**(6), 855-870. https://doi.org/10.1007/s10409-015-0436-3.

Hoek, E. and Bray, J.W. (2005), "Rock slope engineering", 4th Ed., New York: Spon Press.

Hu, B., Yang, S. and Tian, W. (2019), "Creep-permeability behavior of sandstone considering thermal-damage", *Geomech. Eng*., **18**(1), 71-83. https://doi.org/10.12989/gae.2019.18.1.071.

Ibishi, G., Genis, M. and Yavuz, M. (2022), "Post-pillars design for safe exploitation at Trepca hard rock mine (Kosovo) based on numerical modeling", *Geomech. Eng*., **28**(5), 463-475. https://doi.org/10.12989/gae.2022.28.5.463.

Jiang, Q., Liu, X., Wei, W. and Zhou, C. (2013), "Wedge stability analysis for rock slope and search for critical slip surfaces", *Chinese J. Rock Mech. Eng*., **32**(1), 24-33.

Karatela, E. and Taheri, A. (2018), "Three-dimensional hydro-mechanical model of borehole in fractured rock mass using discrete element method", *J Nat Gas Sci Eng*., **53**, 263-275. https://doi.org/10.1016/j.jngse.2018.02.032.

Katcoff, C.Z. and Graham-Brady, L.L. (2014), "Modeling dynamic brittle behavior of materials with circular flaws or pores", *Int. J. Solids Struct*., **51**(3-4), 754-766. https://doi.org/10.1016/ j.ijsolstr.2013.11.004.

Kim, E., Garcia, A. and Changani, H. (2018), "Fragmentation and energy absorption characteristics of Red, Berea and Buff sandstones based on different loading rates and water contents", *Geomech. Eng*., **4**(2), 151-159. https://doi.org/10.12989/gae.2018.4.2.151.

Kim, J.S., Kim, G.Y., Baik. M.H., Finsterle, S. and Cho, G.C. (2019), "A new approach for quantitative damage assessment of in-situ rock mass by acoustic emission", *Geomech. Eng*., **18**(1), 11-20. https://doi.org/10.12989/gae.2019.18.1.011.

Komurlu, E., Kesimal, A. and Demir, S. (2016), "Experimental and numerical analyses on determination of indirect (splitting) tensile strength of cemented paste backfill materials under different loading apparatus", *Geomech. Eng*., **10**(6), 775-791. https://doi.org/10.12989/ gae.2016.10.6.775.

Kumsar, H., Aydan, O. and Ulusay, R. (2000), "Dynamic and static stability assessment of rock slopes against wedge failures", *Rock Mech. Rock Eng.,* **33**(1), 31-51. https://doi.org/10.1007/s006030050003.

Lawal, A.I., Kwon, S., Aladejare, A.E. and Oniyide, G.O. (2022), "Prediction of the static and dynamic mechanical properties of sedimentary rock using soft computing methods", *Geomech. Eng*., **28**(3), 313-324. https://doi.org/10.12989/gae.2022.28.3.313.

Li Z., Dou L., Lu, Z., Lu, X. and Wang, G. (2010), "Study of the fault slide destabilization induced by coal mining", *J. Min. Saf. Eng*., **27**(4), 499-504.

Li, L.P., Chen, D.Y., Li, S.C., Shi, S.S., Zhang, M.G. and Liu, H.L. (2017), "Numerical analysis and fluid-solid coupling model test of filling-type fracture water inrush and mud gush", *Geomech. Eng*., **13**(6), 1011-1025. https://doi.org/10.12989/gae.2017.13.6.1011.

Li, X.B., Feng, F., Li, D.Y., Du, K., Ranjith, P.G. and Rostami, J. (2018), "Failure characteristics of granite influenced by sample height-to-width ratios and intermediate principal stress under true-triaxial unloading conditions", *Rock Mech. Rock Eng*., **51**, 1321-1345. https://doi.org/10.1007/s00603-018-1414-4.

Li, Z., Dou, L., M, Z., Cao, A. and Gong, S. (2008), "Effect of fault on roof rock burst", *J. Min. Saf. Eng*., **25**(2), 154-163.

Lisjak, A. and Grasselli, G. (2014), "A review of discrete modeling techniques for fracturing processes in discontinuous rock mass", *J. Rock Mech. Geotech. Eng*., **6**(4), 301-314. https://doi.org/10.1016/j.jrmge.2013.12.007.

Liu, C., Huang, B., Chang, X., Wang, J. and Wei, M. (2008), "Study on tip to face coal and rock stability control of fully mechanized stepped large cutting height mining in extremely soft thick seam", *J. China Univ. Min. Technol*., **37**(6), 734-739.

Lv, H.Y., Tang, Y.S., Zhang, L.F., Cheng, Z.B. and Zhang, Y.N. (2019), "Analysis for mechanical characteristics and failure models of coal specimens with non-penetrating single crack", *Geomech. Eng*., **17**(4), 355-365. https://doi.org/10.12989/gae.2019.17.4.355.

Mahmoodzadeh, A., Mohammadi, M., Abdulhamid, S., Nariman, A., Hunar, Farid Hama; Ibrahim, Hawkar Hashim; Rashidi, Shima(2022), "Forecasting tunnel path geology using Gaussian process regression", *Geomech. Eng*., **28**(4), 359-374, https://doi.org/10.12989/gae.2022.28.4.359.

Maruvanchery, V. and Kim, E. (2017), "Effects of water on rock fracture properties: Studies of mode I fracture toughness", crack propagation velocity, and consumed energy in calcite-cemented sandstone", *Geomech. Eng*., **17**(1), 57-67. https://doi.org/10.12989/gae.2019.17.1.057.

Meng, Z., Peng, S. and Li, H. (2001), "Changes of the physical and mechanical properties of normal fault near coal and its influence on the rock pressure distribution", *J. China Coal Soc*., **26**(6), 561-566.

Morgan, S.P. and Einstein, H.H. (2017), "Cracking processes affected by bedding planes in Opalinus shale with flaw pairs", *Eng. Fract. Mech*., **176**, 213-234. https://doi.org/10.1016/ j.engfracmech.2017.03.003.

Rastegarnia, A., Ghafoorri, M., Moghaddas, N.H., Lashkaripour, G.R. and Shojaei, H. (2022), "Application of cuttings to estimate the static characteristics of the dolomudstone rocks", *Geomech. Eng*., **29**(1), 65-77. https://doi.org/10.12989/gae.2022.29.1.065.

Samanta, M., Punetha, P. and Sharma, M. (2018), "Effect of roughness on interface shear behavior of sand with steel and concrete surface", *Geomech. Eng*., **14**(4), 387-398.

https://doi.org/10.12989/gae.2018.14.4.387.

Sammis, C.G. and Ashby, M.F. (1986), "The failure of brittle porous solids under compressive stress states", *Acta Metall.*, **34**(3), 511-526. https://doi.org/10.1016/0001-6160(86)90087-8.

Shi Genhua (1981) "Geometrical approach of rock mass stability analysis", *Science in China*, (4), 487-495.

Shi, G. (1977), "Stereographic method of stability analysis of rock mass", *Science in China*, (3), 269-271.

Tasdemir, M.A., Maji, A.K. and Shah, S.P. (1989), "Crack propagation in concrete under compression", *J. Eng. Mech.*, **116**(5), 1058-1076. https://doi.org/10.1061/(asce)0733-9399(1990)116:5(1058).

Vaziri, M.R., Tavakoli, H. And Bahaaddini, M. (2022), "2D numerical study of the mechanical behaviour of non-persistent jointed rock masses under uniaxial and biaxial compression tests", *Geomech. Eng.*, **28**(2), 117-133. https://doi.org/10.12989/gae.2022.28.2.117.

Wang, J., Liu, H. and Li, T. (2007), "Study on numerical simulation of dynamic risk regionalization during exploitation approaching to faults", *Chinese J. Rock Mech. Eng.*, **26**(1), 28-35.

Wang, J., Yang, Y. and Kong, D. (2016), "Failure mechanism and control technology of Longwall coal face in large-cutting-height mining method", *Int. J. Min. Sci. Technol.*, **26**(1), 111-118. https://doi.org/10.1016/j.ijmst.2015.11.018.

Wang, Q., Gao, H., Yu, H., Jiang, B. and Liu, B. (2019), "Method for measuring rock mass characteristics and evaluating the grouting-reinforced effect based on digital drilling", *Rock Mech. Eng. Rock*, **52**(3), 841-851. https://doi.org/10.1007/s00603-018-1624-9.

Xiao, G.F. and Chen, C.X. (2018), "Simulation of progressive failure process and stability analysis method for rock block", *Rock Soil Mech.*, **39**(8), 292-301. https://doi.org/10.16285/j.rsm.2017.2428.

Xing, H.L., Makinouchi, A. and Mora, P. (2007), "Finite element modeling of interacting fault systems", *Physics of the Earth Interiors Planetary*, **163**(1-4), 106-121. https://doi.org/10.1016/j.pepi.2007.05.006.

Xing, H.L., Yu, W. and Zhang, J. (2009), "3D mesh generation in geocomputing", Chapter II in Advances in Geocomputing, Springer-Verlag GmbH, 27-64. https://doi.org/10.1007/978-3-540-85879-9_2.

Xue, Y.C., Sun, W.B. and Wu, Q.S. (2020), "The influence of magmatic rock thickness on fracture and instability law of mining surrounding rock", *Geomech. Eng.*, **20**(6), 547-556. https://doi.org/10.12989/gae.2020.20.6.547.

Yang, J., Zuo, J., Sun, K., Meng, B. and Lin, X.(2011),. "In-situ observation and numerical analysis of surface subsidence of high working face with multi-fault induced by fully mechanized mining activity", *Chinese J. Rock Mech. Eng.*, **30**(6), 1216-1224. https://doi.org/10.1007/s12583-011-0163-z.

Yang, P., Liu, C. and Wu, F. (2012), "Breakage and falling of a high coal face in a thick mined seam", *J. China Univ. Min. Technol.*, **41**(3), 372-377. https://doi.org/10.1007/s11783-011-0280-z.

Yossef, H.H. (2003), "Keyblock stability in seismically active rock slopes—Snake Path Cliff", *Masada. J. Geotech. Geoenviron. Eng.*, **129**(8), 697-705. https://doi.org/10.1061/(ASCE)1090-0241(2003)129:8(697).

Yuan, Y., Tu, S., Ma, X., Sun, L. and Bai, Q. (2012), "Coal wall stability of fully mechanized working face with great mining height in"three soft" coal seam and its control technology", *J. Min. Saf. Eng.*, **29**(1), 21-25.

Zhao, J., Chen, J., Xing, H., Zhihao, Z. and Zhang, X. (2022a), "Dynamic mechanical response and movement evolution characteristics of fault systems in the coal mining process", *Pure Appl. Geophys.*, https://doi.org/10.1007/s00024-021-02905-w

Zhao, J., Liu, Q., Jiang, C. and Wang, D. (2022b), "Application of rock mass index in the prediction of mine water inrush and grouting quantity", *Geomech. Eng.*, **30**(6), 503-515. https://doi.org/10.12989/gae.2022.30.6.503.

Zhao, J.H., Jiang, N., Yin, L.M. and Bai, L.Y. (2018), "The effects of mining subsidence and drainage improvements on a waterlogged area", *Bull. Eng. Geol. Environ.*, **78**(5), 3815-3831. https://doi.org/10.1007/ s10064-018-1356-9

Zhao, J.H., Yin, L.M. and Guo, W.J. (2018), "Stress– seepage coupling of cataclastic rock masses based on digital image technologies", *Rock Mech. Rock Eng.*, **51**(8), 2355-2372. https://doi.org/10.1007/s00603-018-1474-5.

Zhou, F., Sun, W.B., Shao, J.L., Kong, L.J. and Geng, X.Y. (2020), "Experimental study on nano silica modified cement base grouting reinforcement materials", *Geomech. Eng.*, **20**(1), 67-73. https://doi.org/10.12989/gae.2020.20.1.067.

CC